JMEPEG (2018) 27:4799–4809
https://doi.org/10.1007/s11665-018-3579-0

1059-9495/$19.00

Surface Modification of 304 Stainless Steel by Electro-Spark Deposition

Z. Jiao, S. Peterkin, L. Felix, R. Liang, J.P. Oliveira, N. Schell, N. Scotchmer, E. Toyserkani, and Y. Zhou

(Submitted September 4, 2017; in revised form May 19, 2018; published online August 20, 2018)

Electro-spark deposition (ESD) is a pulsed microwelding process that is used to apply surface coatings for the repair of damaged high value and precision products or modify their surfaces for specific properties. The low heat input, minimal heat-affected zone and the ability to form metallurgical bonding of coating to substrate are major advantages of the ESD process. Many applications require the components to have excellent surface performance, such as wear and corrosion resistance. ESD technique provides an approach to modify the component surface without compromising the bulk properties. In this study, surface modifications of 304 stainless steel by ESD were investigated. Titanium carbide (TiC), tungsten carbide (WC) and molybdenum (Mo) were employed as coating materials. Scanning electron microscopy (SEM) and energy-dispersive x-ray spectroscopy (EDX) analysis were conducted to characterize the microstructure and composition of the coatings. The coatings thicknesses were all around 40 µm. The results showed that TiC and WC coatings showed a dramatic increase in the microhardness, up to 5 times. WC coating improved the wear resistance by more than 5 times, while TiC and Mo coatings also improved it by approximately 2.5 times. Electro-chemical tests were conducted to investigate the corrosion resistance of the coatings. Mo coating exhibited a significant improvement in the corrosion resistance in 5% NaCl solutions, corroding 350 times slower than stainless steel. Synchrotron x-ray diffraction was performed to investigate the microstructure changes of the Mo-coated sample. Heat treatment was also carried out to investigate the corrosion behavior of Mo-coated 304 stainless steel at elevated service temperature in air or argon.

Keywords corrosion resistance, electro-spark deposition, stainless steel, surface modification

1. Introduction

Electro-spark deposition is a micro-welding process that uses short-duration electrical pulses to deposit electrode materials onto conductive substrates. ESD is increasingly used to repair damaged high-value precision products or modify their surfaces to attain specific properties (Ref 1). Various coating material and substrate pairings have been studied to locally improve properties, such as wear resistance, corrosion resistance and hardness (Ref 2-6). ESD is considered a more environmentally friendly process when compared to previously used coating processes employing hazardous chemicals such as hard chromium plating. ESD is able to apply coatings with metallurgical bond to the substrates, which ensures excellent adhesion with high spalling resistance. In addition, ESD has low heat input which minimizes the heat-affected zone, thermal damage and impact on the substrate material (Ref 7). The bulk substrate remains close to ambient temperature due to the nature of the deposition process.

Stainless steel is an ideal material where the properties of steel paired with corrosion resistance are required. Stainless steels contain sufficient chromium to form a passive layer of chromium oxide, which prevents further surface corrosion into the metal's internal structure. Various alloy elements are added into stainless steel to tune its microstructure and properties. Stainless steel has numerous applications and wide appeal in household hardware, surgical instruments, appliances, industrial equipment, automotive manufacturing and as structural aerospace alloys. In some applications, the performance of the stainless steel components can be improved by altering the local properties, such as corrosion resistance, wear resistance and hardness.

The ESD technique provides a feasible approach to apply coating materials. Previous research studied ESD of hard cermet coatings to obtain better surface properties. For example, Wang et al. (Ref 8) applied WC coating on spheroidal graphite roll substrate by ESD. The coating exhibited tripled microhardness and doubled wear resistance compared to the base metal. Tkachenko et al. (Ref 9) investigated ESD of TiC coating on steel 45, and the results indicate the coating improved the wear resistance more than three times. Investi-

Electronic supplementary material The online version of this article (https://doi.org/10.1007/s11665-018-3579-0) contains supplementary material, which is available to authorized users.

Z. Jiao, Centre for Advanced Materials Joining, University of Waterloo, Waterloo, ON N2L 3G1, Canada; Department of Mechanical and Mechatronics Engineering, University of Waterloo, Waterloo, ON N2L 3G1, Canada; and Huys Industries Ltd., 175 Toryork Drive, Unit 35, Weston, ON M9L 1X9, Canada; **S. Peterkin** and **N. Scotchmer**, Huys Industries Ltd., 175 Toryork Drive, Unit 35, Weston, ON M9L 1X9, Canada; and **L. Felix, R. Liang,** and **Y. Zhou**, Centre for Advanced Materials Joining, University of Waterloo, Waterloo, ON N2L 3G1, Canada; and Department of Mechanical and Mechatronics Engineering, University of Waterloo, Waterloo, ON N2L 3G1, Canada; and **J. P. Oliveira**, Department of Materials Science and Engineering, The Ohio State University, 1248 Arthur E. Adams Drive, Columbus, OH 43221; and **N. Schell**, Institute of Materials Research, Helmholtz-Zentrum Geesthacht, Max-Planck-Str. 1, 21502 Geesthacht, Germany; and **E. Toyserkani**, Department of Mechanical and Mechatronics Engineering, University of Waterloo, Waterloo, ON N2L 3G1, Canada. Contact e-mail: berryfoss@gmail.com.

gation into surface modification of stainless steel can obtain better surface performance without compromising the bulk material properties and thus open new applications for stainless steel. The microstructure and composition of stainless steels are tuned to meet specific application requirements. Duplex stainless steels have a mixed microstructure of 50% austenite and 50% ferrite, which provides better strength and higher corrosion resistance compared to normal austenitic stainless steels (Ref 10). They also contain high chromium (19-32 wt.%) and molybdenum (up to 7 wt.%) and lower nickel than austenitic stainless steels. As a result of the additional alloying elements and processing requirements, duplex stainless steels carry a higher cost when compared to the traditional austenitic stainless steels. The cost of a duplex stainless steel component would be proportionately higher to achieve higher corrosion resistance and strength. In many applications, high corrosion resistance is only required in some localized areas. Applying a high corrosion resistance coating on a given localized area could be an effective and economical choice. Madjid et al. (Ref 11) applied Mo coating on 316 stainless steel using nitrogen ion implantation. The results showed improved corrosion resistance in acid solutions.

In this work, we report the approach to the surface modification of 304 stainless steel by electro-spark deposition. Microstructures of TiC-, WC- and Mo-coated 304 stainless steel are investigated and their properties such as microhardness, wear resistance and corrosion resistance evaluated. The corrosion behavior of Mo-coated 304 stainless steel after heat treatment is also discussed. These results demonstrate the potential of the ESD technique and can enable the exploration of new applications using ESD-coated 304 stainless steel.

2. Experiment

The ESD equipment was provided by Huys Industries Ltd. and modified at the Center of Advance Materials Joining (CAMJ) at the University of Waterloo. The ESD apparatus has a control panel to set the electrical parameters including spark voltage (20-150 V), capacitance (10-310 μF) and frequency (64-500 Hz). In this study, all ESD coatings were manually deposited while locally shielded by ultra-pure argon gas. The coating material is deposited via a handheld applicator, which transfers the electrical signals and facilitates relative motion through the use of rotation to prevent the electrode sticking to the substrate surface.

The substrate material, 304 stainless steel, thickness 1.2 mm, was supplied by McMaster Carr. TiC, WC and Mo electrodes used in this study were supplied by TechnoCoat Co., Ltd., Japan. The diameters of these electrodes were 3 mm in all cases. The TiC electrode contains approximately 5% of nickel (Ni), and the WC electrode contains around 5% cobalt (Co) as binding materials.

Electrical parameters, such as spark voltage, capacitance and frequency, are critical for successful ESD coatings. When the spark energy is low, no coating was found on the substrate surface since the spark energy was insufficient to melt the electrode material. When the electrical parameters resulted in excessive spark energy, the electrode would overheat which could form burnt depositions or big chunk of un-bonded molten metal. The optimized parameters may vary significantly for different material combinations. A series of experiments were performed to determine the processing window for depositing TiC, WC and Mo on 304 stainless steel by ESD. The resultant operation window for these three coatings is listed in Table 1. Within the process window, 6 sets of parameters are tested for each combination. Cross-sectional analysis was carried out to find the optimized parameter based on the coating microstructure. The coating with less crack and porosity was considered as the optimized parameter. The optimized parameter used in this study is listed in Table 1. The deposition time for these three coatings was maintained at 30 s per cm^2.

The microstructure of the coated samples was analyzed by SEM, using a JEOL JSM 6460. EDX analysis was performed with an INCA-350 from Oxford Instruments for elemental characterization. Vickers microhardness profiles were obtained using a Wilson Vickers 402MVD automated hardness tester with 100-g load and 15-s dwell time, following the ASTM E384-16 standard. Five repeated tests were performed for every specific area. Wear resistance test was conducted as per the ASTM-G65-04 standard (measuring abrasion using the dry sand/rubber wheel) using Procedure C. This test is used to evaluate the resistance to scratching abrasion under a specified set of conditions. In this study, the wear resistance was evaluated by mass loss of the tested specimen. The abrasive used was Ottawa silica sand in a 50/70 mesh size (particle size is 212-300 μm in diameter) with an angular morphology. The samples were ultrasonically degreased in ethanol and rinsed with deionized water before the wear resistance test. Procedure C requires 100 revolutions of the abrasive wheel with a 130-N load. Five repeated tests were performed for each sample. Electro-chemical tests were performed using a Gamry Series G300 Potentiostat to evaluate corrosion resistance of the sample. In this study, an Ag/AgCl electrode was employed as the reference electrode due to its stable, well-defined electrochemical potential. Pure platinum wire was used as the counter electrode, and the sample was set up as the working electrode. Bubbling nitrogen was introduced to the electro-chemical cell to remove oxygen from the test solution. The solution used for all the electro-chemical tests in this study was 5% NaCl. The size of the testing samples was 9 mm by 9 mm. Synchrotron x-ray diffraction was performed at beamline P07 high energy materials science (HEMS) of PETRA III/DESY on Mo-coated sample. The sample was positioned at 1440 mm from the 2D MAR345 detector, and the wavelength used was of 0.14235 A (87 keV). Fit2D (Ref 12) was used to analyze the raw diffraction images and convert them into intensity versus interplanar spacing plots similarly to (Ref 13, 14). Regular XRD analyses were conducted with PANalytical X'Pert PRO MPD equipment. Copper k-alpha x-ray source was generated with 1.54 Å wavelength. The heat treatment of Mo-coated samples was performed in a tube furnace. The samples were heated up to 400 and 650 °C and kept at the elevated temperature for 1 h. One set of the samples was heat-treated in air, and the other set in argon shielding gas. All samples were cooled down to room temperature inside the furnace.

3. Results and Discussion

3.1 Elemental Analysis

Figure 1(a) shows the SEM images of the TiC-coated 304 stainless steel. Limited porosity was observed in the TiC

Table 1 Operation window of TiC, WC and Mo coating on stainless steel by ESD

Coating	TiC	WC	Mo
Operation window	35 V, 280-300 μF, 75-150 Hz 85 V, 100-150 μF, 120-360 Hz 135 V, 10-30 μF, 120-260 Hz	35 V, 100-300 μF, 150-480 Hz 85 V, 40-150 μF, 150-480 Hz 135 V, 10-40 μF, 120-480 Hz	35 V, 150-300 μF, 120-260 Hz 85 V, 40-300 μF, 120-360 Hz 135 V, 10-120 μF, 120-360 Hz
Optimized parameters	85 V, 120 μF, 260 Hz	85 V, 100 μF, 260 Hz	85 V, 150 μF, 260 Hz

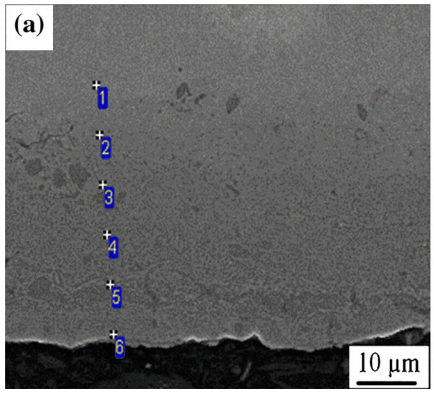

(b)

Spectrum	Ti	Cr	Fe	Ni
1		21.63	71.92	6.46
2	29.44	13.91	49.69	6.97
3	44.96	10.34	36.45	8.26
4	58.01	7.36	21.86	12.76
5	78.96	2.61	8.76	9.66
6	79.65	2.44	8.02	9.88

Fig. 1 SEM and EDX results of TiC-coated stainless steel. (a) The points indicate testing location, (b) corresponding composition data in wt.%

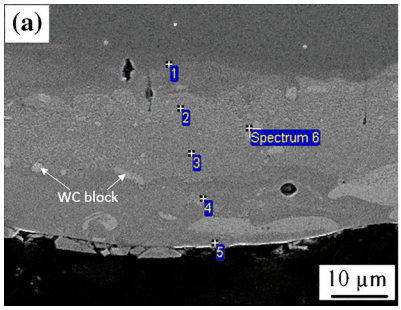

(b)

Spectrum	Cr	Fe	Ni	W
1	19.43	62.36	5.20	13.01
2	8.65	32.21	5.22	53.92
3	10.33	41.34	3.38	44.95
4	9.06	35.26	5.49	50.19
5	10.14	36.88	7.40	45.57
6				100.00

Fig. 2 SEM and EDX results of WC-coated stainless steel. (a) The points indicate testing location, (b) corresponding composition data in wt.%

coatings. No major cracks were found at the interface between the coating and the stainless steel substrate. Figure 1(b) shows EDX results of TiC-coated 304 stainless steel, and the figures represent the percentages by weight (wt.%). The points in Fig. 1(a) indicate the testing location, and Fig. 1(b) shows the corresponding compositional data. The figures show that the Ti content increases with the coating thickness, while the compositional elements of the substrate decrease. There is very little iron (Fe) content on the coating surface, demonstrating the barrier effect of the TiC coating to reduce stainless steel diffusing. The TiC coating thickness was approximately 40 μm.

Figure 2(a) shows the microstructure of a WC coating on 304 stainless steel. It shows few porosities and small transverse cracks. The EDX results, shown in Fig. 2(b), indicate that considerable amounts of Fe were present on the coating surface. The color variations in the WC coating also indicate that the coating composition is not uniform. There are some bright areas in the WC coating, and spectrum 6 indicates that the bright area is pure WC. Similar results were obtained in a previous research of ESD of WC on low carbon steel (Ref 15). It is suggested that the electrode material and substrate material are randomly mixed together. The heat generated in the ESD process could melt the binding material, but cannot effectively melt and distribute the WC. As a result, many WC blocks were found in the coating.

Figure 3 shows the SEM image of a Mo coating on 304 stainless steel. It should be noted that the Mo content is relatively constant from the coating surface into the substrate. The coating is quite uniform, and no major cracks or porosities are to be seen. From the phase diagram, Mo can easily react with Fe and Cr to form various alloys. ESD of Mo on 304 stainless steel can be considered as a surface alloying process.

3.2 Mechanical Properties

Microhardness test results are shown in Fig. 4. The plots display the microhardness change with the distance from coating surface. The comparison of the average coating hardness to the base metal results is shown in Table 2. The

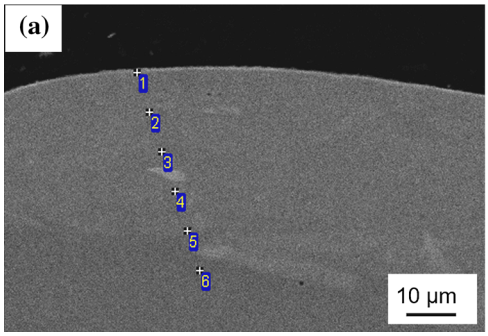

(b)

Spectrum	Cr	Fe	Mo	Ni
1	11.01	51.64	32.03	5.32
2	9.51	51.25	34.98	4.26
3	10.55	50.14	35.92	3.39
4	9.87	47.85	36.18	5.10
5	10.96	63.44	19.74	5.86
6	15.05	76.03		8.92

Fig. 3 SEM and EDX results of Mo-coated stainless steel. (a) The points indicate testing location, (b) corresponding composition data in wt.%

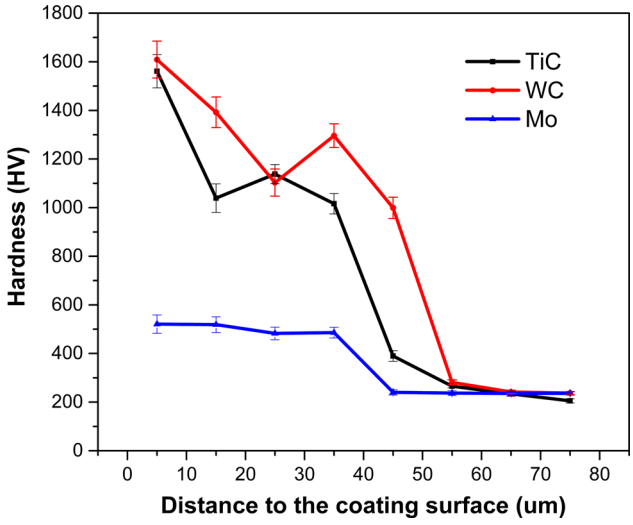

Fig. 4 Microhardness results of coated stainless steel

Table 2 Microhardness of different coatings

HV0.1	TiC	WC	Mo	SS
Average	1188.5	1279.8	502.0	237.5
Standard deviation	52.2	57.6	29.5	9.5
Percentage change to base metal	400%	439%	111%	…

microhardness values of the cermet coatings TiC and WC are increased 4 times more than the hardness of the substrate material. The hardness of the Mo coating is twice that of the base metal.

Wear resistance is another commonly desired surface property. In this study, wear resistance was evaluated by mass loss. Materials with higher wear resistance exhibit lower mass losses. Figure 5 shows wear resistance test results of TiC-, WC- and Mo-coated 304 stainless steels. The quantitative results are listed in Table 3. The quantitative evaluation of the results shows that the WC coating demonstrated the greatest wear resistance which increased 4 times more than the base metal. The TiC and Mo coatings improved the wear resistance by 1.5 times more than 304 stainless steel.

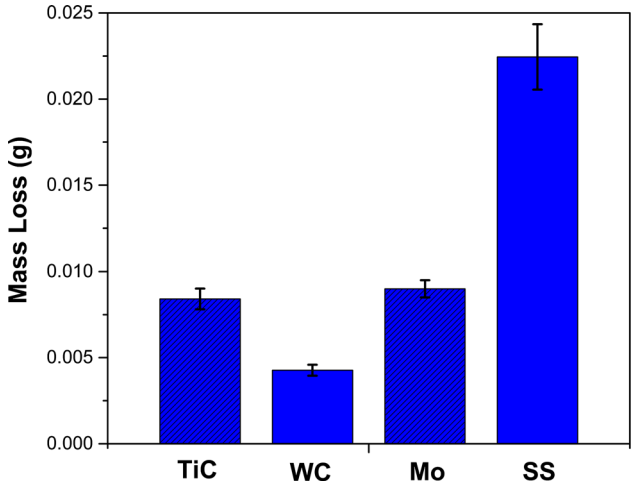

Fig. 5 Wear resistance results of ESD-coated stainless steel

3.3 Corrosion Behaviors

The Tafel test is a commonly used electro-chemical method to evaluate corrosion resistance. Classic Tafel analysis is performed by extrapolating the linear portions of a logarithmic current versus potential plot to determine their intersection. The value of the anodic and cathodic current at the intersection is the corrosion current I_{corr}. The corrosion rate (CR) can then be calculated with Eq 1:

$$CR = \frac{I_{corr} \cdot K \cdot EW}{dA} \quad \text{(Eq 1)}$$

where K is a constant that defines the units for the corrosion rate, EW represents the equivalent weight, d is the density of the material being investigated, and A is the relevant sample area. In this study, Tafel tests were performed for TiC-, WC- and Mo-coated samples in 5% NaCl solution. The Tafel plots are shown in Fig. 6. The corrosion current and voltage are determined by fitting two tangents to the Tafel plot. Ideally, the sample with better corrosion resistance should have a Tafel curve on the top left of the plot. It can be seen from Fig. 6 that the Mo-coated stainless steel has the best corrosion resistance.

The measured corrosion voltage, corrosion current and calculated corrosion rate are listed in Table 4. The unit for corrosion rate is mils per year (mpy), in which a mil equals to a thousandth of an inch. It should be noted that the Mo-coated sample has a much lower corrosion current, which relates to a

Table 3 Mass loss of different ESD-coated stainless steel

Wear resistance	TiC	WC	Mo	SS
Average mass loss, g	8.41×10^{-3}	4.27×10^{-3}	9.00×10^{-3}	2.25×10^{-2}
Standard deviation, g	6.04×10^{-4}	3.26×10^{-4}	5.12×10^{-4}	1.91×10^{-3}
Percentage change to base metal	168%	427%	150%	…

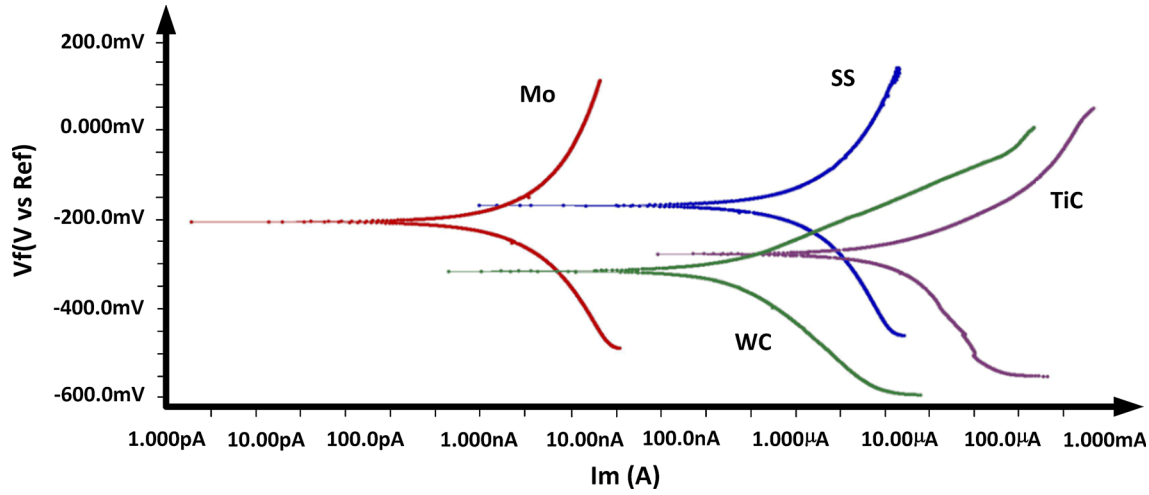

Fig. 6 Tafel test results of ESD-coated samples and stainless steel in 5% NaCl solution

Table 4 Tafel analysis of ESD-coated stainless steel in 5% NaCl solution

Tafel	SS	Mo	TiC	WC
E_{corr}, mV	− 163	− 199	− 272	− 309
I_{corr}, A	2.90×10^{-6}	8.18×10^{-9}	9.39×10^{-6}	2.93×10^{-7}
Corrosion rate, mpy	14.89	4.20×10^{-2}	48.21	1.505

corrosion rate more than 350 times slower than that of the base metal 304 stainless steel. The WC coating exhibits nearly 10 times better corrosion resistance than the base metal. On the other hand, the TiC coating does not show promising results in the corrosion resistance. The corrosion potential of TiC and WC coating is much lower than that of Mo coating and base metal, indicating the corrosion reaction is easier to occur for TiC and WC coatings. The TiC and WC are cermet coatings that have drastically different material properties compared to base metal 304 stainless steel. EDX results from Fig. 1 and 2 also indicate the cermet coatings are not uniform, where some areas could be the weak points to corrosion attacks. However, the Mo content is quite consistent across the Mo coating, as shown in Fig. 3. The more uniform coating contributes to better corrosion resistance of Mo coatings.

According to the ASTM G48 standard (Ref 16), the pitting resistance equivalent number (PREN) is a measurement of the corrosion resistance for various types of stainless steel. The PREN value can be calculated with Eq 2:

$$\mathrm{PREN} = 1 \times \%\mathrm{Cr} + 3.3 \times \%\mathrm{Mo} + 16 \times \%\mathrm{N}, \quad \text{with } x \text{ in wt.\%}. \tag{Eq 2}$$

Therefore, in terms of corrosion resistance, Mo is more effective compared to Cr since it has a 3.3 factor in the equation. Previous research also showed the contribution of Mo to the improvement in corrosion resistance of stainless steel in different solutions (Ref 17-19).

Synchrotron x-ray diffraction (XRD) was used to precisely probe the microstructure of the Mo-coated sample. High-energy synchrotron XRD diffraction has the advantages of high photon flux and fast acquisition rate. It is able to work in transmission mode, and the spot size can be much smaller than traditional XRD. As such, this is an advanced technique for probing processed materials where microstructural modifications occur on a very small scale and thus cannot be distinguished using convention methods. The superimposed patterns obtained using synchrotron XRD on the Mo-coated stainless steel are shown in Fig. 7. The synchrotron XRD was performed on the cross-sectioned sample and scanned from the coating surface to the base metal. It should be noted that only one pattern is indexed in Fig. 7 since these patterns share the same peak locations.

The results show α(220) and α(211) peaks are much stronger in Mo-coated area, while the γ-phase peaks are relatively weaker than that in base metal. The results indicate the phase transformation from austenite to ferrite after the deposition of Mo. Duplex stainless steel is considered as a high corrosion resistance stainless steel due to its 50% austenite/50% ferrite structure (Ref 20). It is suggested that the change of

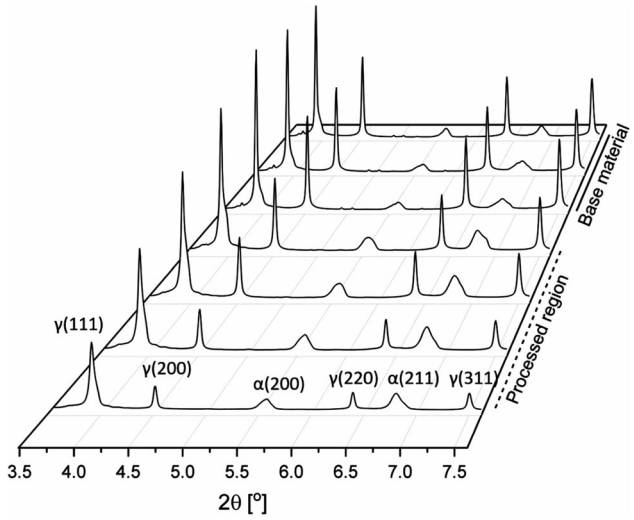

Fig. 7 XRD patterns on different regions of the Mo-coated 304 stainless steel

austenite to ferrite ratio can significantly affect the corrosion behavior of stainless steel. Mo is a ferrite stabilizer, which could facilitate the phase transformation of austenite to ferrite (Ref 21). The phase transformation after Mo deposition contributes to the improvement on the corrosion resistance.

3.4 Corrosion Behavior of Heat-Treated Mo-Coated Stainless Steels

Mo ESD-coated 304 stainless steels have been shown to exhibit improved corrosion resistance to high concentration NaCl solutions. The ESD process, characterized by rapid mass transfer, high cooling rates and low net heat input, results in non-equilibrium coatings. After processing, the coatings often exhibit minimal diffusion and potentially high residual stresses, localized at the part surface. The corrosion performance of the treated parts could be altered by diffusing the highly concentrated Mo coating and promoting the formation of secondary Mo and stainless steel phases (Ref 21). In this section, the as-ESD-coated Mo on stainless steel samples was heat-treated in air and Ar environments, to investigate the corrosion behavior of the coatings with altered microstructures. The samples were treated at 400 and 650 °C, in air and Ar.

Figure 8(a) reports the XRD spectrums for the 304 stainless steel substrate before processing, and the characteristic austenitic and ferritic phase peaks can be observed. Figure 8(b) shows the XRD spectrum for the as-deposited Mo ESD coating on the stainless steel substrate. The results depict an increased peak amplitude for the ferritic phase, with a decrease in the austenitic phase. Mo is known as a ferrite stabilizer, and the diffused Mo coating at the surface of the 304 stainless steel substrate promotes ferrite formation (Ref 21). The ESD process, characterized by the high cooling rates and low heat inputs, localizes the affected area to the surface of the substrate. High concentrations of Mo can be found at the surface, without sufficient heat to promote the diffusion of the Mo into the 304 stainless steel, or the formation of intermetallic phases. Intermetallic phases rapidly form when high temperatures near 850-900 °C are reached (Ref 24). Padgurskasa et al. (Ref 22) also reported no evidence of intermetallic phases in Mo ESD coatings on steels.

Figure 8(c) shows the XRD spectrum of the Mo ESD-coated 304 stainless steel samples after heat treatment in air at 400 °C for 1 h. When compared to the as-deposited XRD spectrums as observed in Fig. 8(b), the austenite peaks at 2θ above 70° have disappeared and the relative intensity of the (200) peak has decreased to an intensity close to 2θ at 51°. For the ferrite and austenite peaks below 2θ 45°, there was an increase in intensity. Two additional peaks for Cr oxide are observed for the heat-treated samples. The Cr oxides are formed at the surface due to the elevated temperatures and exposure to oxygen during the heat treatment process.

Figure 8(d) shows the XRD pattern for the sample heat-treated in Ar at 400 °C for 1 h. Phase transformations from austenite to ferrite are observed, from the increase in the intensity of the ferritic peak. The Cr_2O_3 chrome oxide peaks are relatively lower for the samples heat-treated in Ar versus those treated in air from Fig. 8(c). This supports that the Ar atmosphere was effective in reducing the atmospheric interactions of the sample during heat treatment. The presence of the Cr oxides in the samples heat-treated in Ar may be representative of insufficient shielding in the tube furnace. With less oxidation of the Cr alloy content at the surface, the remaining Cr is able to diffuse with the Mo content and promote additional ferrite stabilization. The ferrite peaks for the samples heat-treated at 400 °C for 1 h in Ar exhibited higher-intensity ferrite peaks when compared to the samples heat-treated in air. No pure Mo peaks are detected in either of the samples heat-treated at 400 °C for 1 h, in air or Ar. The Mo content has diffused into the stainless steel and only remains as a solid solution near the surface.

Figure 8(e) shows the XRD spectrum for the Mo ESD-coated 304 stainless steel after heat treatment at 650 °C for 1 h in air. The high treatment temperature and atmospheric interactions resulted in a significant reduction of the ferrite peaks. The Cr and Mo ferrite stabilizers diffused to the sample surface where they formed oxides by interacting with the atmospheric oxygen content. Figure 8(e) exhibits high-intensity peaks for Mo, Fe and Cr oxides. The results demonstrate that 650 °C in air is above the operating temperature of the Mo ESD coatings, where the alloying elements in the substrate will be depleted due to diffusion and oxidation. 650 °C is within the temperature range for sensitization of stainless steels, where the Cr content at the grain boundaries depletes, due to the formation of Cr carbides (Ref 25). Cr- and Mo-rich phases and carbides can be formed in temperature ranges near 650 °C (Ref 23). Figure 8(e) exhibits the two Mo phase peaks, near 2θ 45° and 60°, and these peaks support the presence of Mo intermetallic phases. The high concentration of Mo after ESD processing promotes the formation of Mo and stainless steel intermetallics during heat treatment.

Figure 8(f) displays the XRD spectrum for the Mo ESD-coated samples heat-treated at 650 °C for 1 h in Ar. Similar to the tests done at 400 °C in air and Ar, the shielded samples exhibited higher ferrite content. The Cr content in the stainless steel and the added Mo both serve to stabilize the ferrite phases of the stainless steel (Ref 26). The inert atmosphere serves to reduce the oxidation reactions which would deplete the Cr and Mo content near the surface of the samples. The formation of intermetallic phases can be enhanced by a depletion in ferrite stabilizers (Ref 27). The Mo metallic phase peak can indicate the presence of Mo stainless steel intermetallic phases.

Figure 3(a), the as-deposited Mo ESD coating, shows a uniform coating, with minimal defects, cracks and pores. The

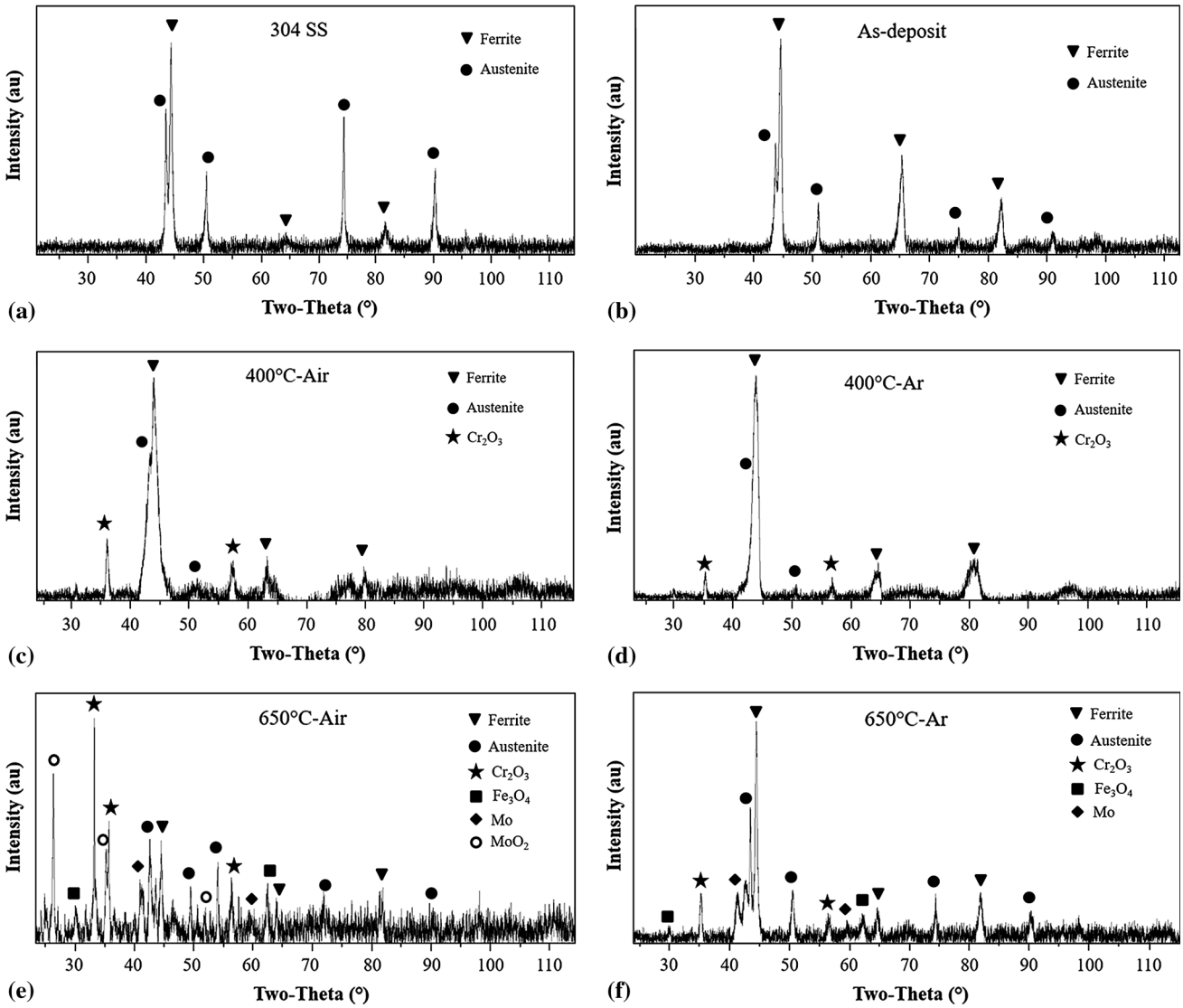

Fig. 8 XRD patterns of samples: (a) 304 stainless steel, (b) as-deposited Mo-coated stainless steel, (c) 400 °C heat-treated in air, (d) 400 °C heat-treated in Ar, (e) 650 °C heat-treated in air, (f) 650 °C heat-treated in Ar

EDX results in Fig. 3(b) show the thickness of the coating from the sampling points 1-4, from the surface to the bulk of the substrate, and there is a high and consistent Mo content. Approximately 50 µm (EDX point 6) into the substrate, the EDX results show that there is a sudden drop off in Mo content, demonstrating that the ESD Mo coating is a mixture of the Mo and stainless steel in the processed zone. Figure 9 displays the SEM images and corresponding EDX results at different areas of interest on the sample cross sections. Figure 9(a) displays the SEM cross-sectional images of a sample heat-treated in air at 400 °C for 1 h in air. The EDX results in Fig. 9(b) report that a high concentration of Mo remains near the sample surface. The points of interest 1 and 3 report higher Mo content than the as-deposited ESD coating concentrations. The Mo content then drops off to 15% at approximately 60 µm. The heat treatment has resulted in Mo-rich zones due to the diffusion of the originally uniform 30% Mo concentration to congregate in lower-energy locations. Additionally, the XRD results indicated that the heat treatments in air resulted in higher oxide concentrations at the surface, including Mo oxides. The coating is now more clearly visible indicating a possible segregation of the Mo content, with some cracks visible near the interface of the high Mo content region.

Figure 9(c) shows the SEM images of the sample heat-treated at 400 °C for 1 h in an Ar atmosphere. Figure 9(d) shows the EDX results for the points of interest on the sample cross section. These results show that there is now Mo content of 16% up to 90 µm (point 5) from the surface, indicating a significant diffusion of the Mo content toward the bulk of the stainless steel substrate. Closer to the surface, points 2 and 3 indicate Mo content up to 75% supporting that there is a significant segregation of Mo content due to diffusion. These regions have depleted Cr and steel content, and segregation of the alloying content will reduce the corrosion performance of the coatings. The SEM image appears to show fewer cracks at the coating interface, and the coating better resembles the as-deposited condition, when compared to the sample heat-treated in air.

Figure 9(e) and (f) shows the SEM and EDX results, respectively, for the Mo-coated sample heat-treated in air at

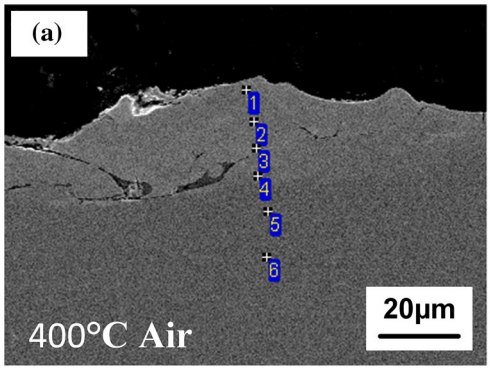

(b)

Spectrum	Cr	Fe	Mo	Ni
1	6.15	45.65	40.15	4.72
2	10.40	53.73	30.24	5.63
3	7.67	38.91	49.22	4.20
4	12.44	65.92	15.10	6.54
5	18.02	72.16		9.82
6	14.16	74.65	1.98	9.21

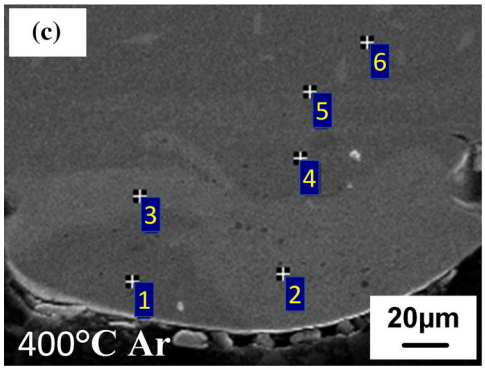

(d)

Spectrum	Cr	Fe	Mo	Ni
1	13.43	58.66	20.35	7.56
2	3.72	22.92	71.02	2.34
3	2.56	21.13	74.21	2.10
4	14.70	66.78	11.54	6.98
5	13.18	62.04	16.11	8.67
6	15.86	73.26	1.03	9.85

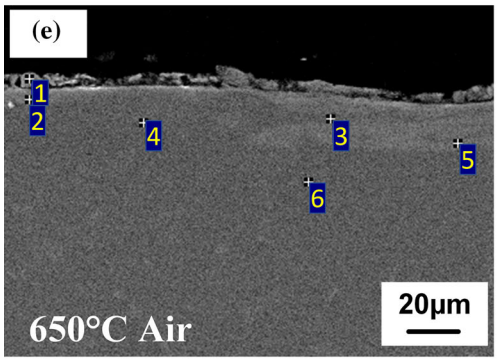

(f)

Spectrum	Cr	Fe	Mo	Ni
1	6.83	41.68	48.87	2.62
2	7.17	45.33	43.12	4.38
3	16.13	63.32	10.05	10.50
4	13.97	69.18	8.30	8.55
5	9.41	62.17	23.06	5.36
6	17.03	73.76		9.21

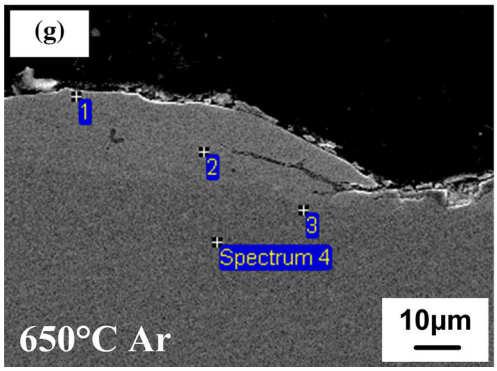

(h)

Spectrum	Cr	Fe	Mo	Ni
1	11.50	54.80	27.74	5.96
2	7.42	45.77	42.19	4.62
3	12.46	77.82	0.12	9.60
4	16.32	73.42	0.85	9.41

Fig. 9 SEM and EDX results for Mo-coated samples: (a) and (b) heat-treated at 400 °C in air, (c) and (d) heat-treated at 400 °C in Ar, (e) and (f) heat-treated at 650 °C in air, (g) and (h) heat-treated at 650 °C in Ar

650 °C for 1 h. The coating thickness has decreased to approximately 15 μm, and some debris, likely fractured oxides and carbides layers are present at the surface. As before there are localized areas with high Mo content. The increased energy for diffusion promotes the migration of Mo into the bulk of the stainless steel, the formation of Mo-rich areas and the formation of Mo oxides at the surface. Figure 9(g) and (h) shows that the SEM and EDX results, respectively, for the sample heat-treated in Ar at 650 °C for 1 h, do not show a significant improvement to the results shown in Fig. 9(e) and (f). Damage to the coating surface can be seen, indicating some oxide formation during heat treatment. Some cracks are now present in the coating, the coating thickness is greatly reduced, and there are localized high Mo concentration areas.

Figure 10 and 11 present the Tafel test results which relate to the corrosion resistance properties of the coatings. The as-deposited Mo ESD coating on 304 stainless steel was compared to coatings which were heat-treated at 400 and 650 °C as well as in air or in Ar atmospheres. The heat-treated samples all resulted in reduced corrosion resistance properties when compared to the as-deposited coating.

The SEM images and EDX results in Fig. 9 demonstrated that the heat-treated samples exhibited cracks and debris after heat treatment. These cracks can activate corrosion mechanisms like crevice corrosion leading to accelerated deterioration of the coated surface. The consolidation of Mo-rich zones depletes the matrix of the alloying elements leaving areas weakened to corrosion. The XRD results shown in Fig. 8 reported that the heat treatments increased the Mo and Cr oxides at the surface. These oxides reduce the Mo and Cr content in the coating and reduce the corrosion resistance (Ref 23). These changes to the coating all contribute to the lower corrosion resistance of the heat-treated samples, when compared to the as-deposited coating. The results for the Tafel tests are summarized in Table 5.

The Tafel test results in Fig. 10, 11 and Table 5 indicate that the samples heat-treated at 650 °C for 1 h had the lowest corrosion resistance. The degradation of the coating properties at high temperatures contributes to the poor performance. The formation of intermetallic phases in the vicinity of Cr-depleted

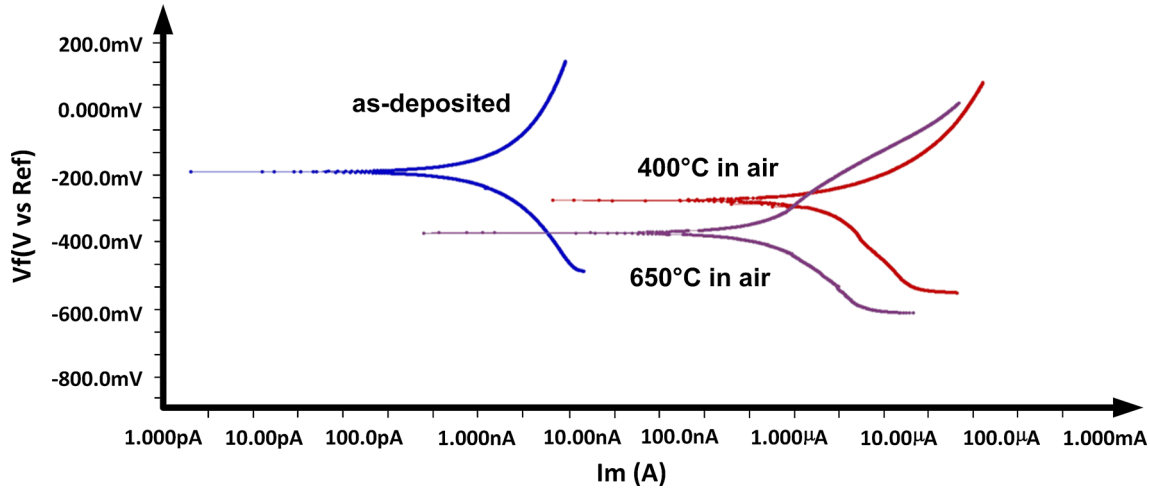

Fig. 10 Tafel test of heat-treated samples in air and Mo-coated 304 SS

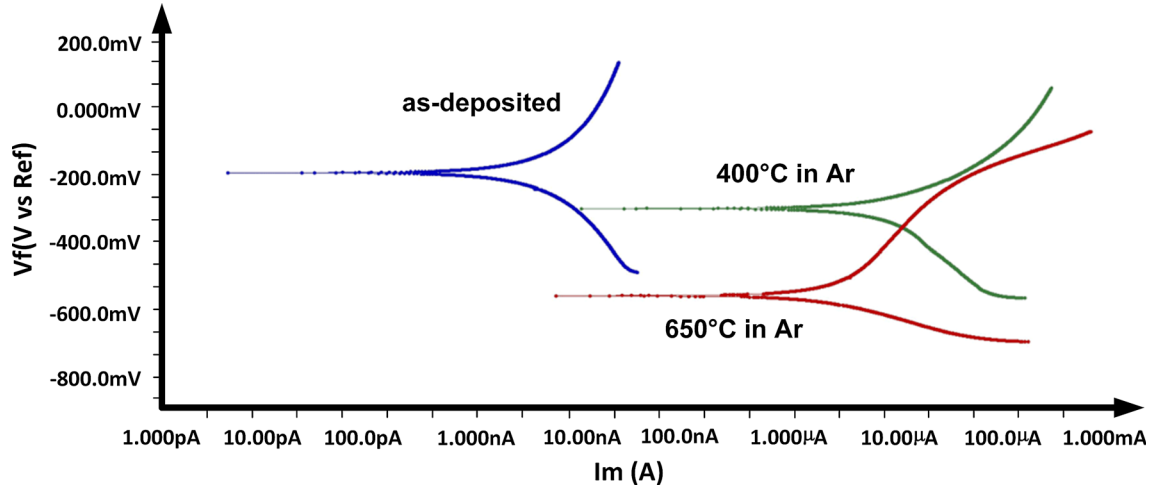

Fig. 11 Tafel test of heat-treated samples in Ar and Mo-coated 304 SS

Table 5 Tafel test results of heat-treated samples and Mo-coated SS

	Mo	400 °C (air)	400 °C (Ar)	650 °C (air)	650 °C
E_{corr}, mV	− 199	− 281	− 301	− 374	− 550
I_{corr}, A	8.18×10^{-9}	6.98×10^{-6}	8.88×10^{-6}	3.70×10^{-6}	2.10×10^{-6}
Corrosion rate, mpy	4.20×10^{-2}	35.96	45.73	19.05	10.80

stainless steel matrix zones is susceptible to pitting corrosion due to weakened passivation (Ref 28). The precipitation of Cr and Mo intermetallic at the grain boundaries of the stainless steel can also lead to an increase in intergranular corrosion (Ref 24). Notably, the change in surface roughness and the formation of cracks at the high-temperature heat treatments can contribute to the lowered corrosion resistance.

Throughout the experiments the Ar shielding was shown to mitigate some of the negative effects of heat treatment in air at all temperatures, such as reducing the oxide concentration, as shown in the XRD results. The Tafel test results showed that at 650 °C the Ar-shielded samples had improved corrosion resistance; however, at 400 °C the effect was reversed. While the Ar shielding is clearly shown to reduce the negative effects of the heat treatments in air, the effect does not always result in improved corrosion resistance.

4. Conclusions

The study reported in this paper describes experiment about the surface modification of 304 stainless steel with the ESD process. The microstructure and performance of the TiC, WC and Mo coatings on stainless steel were discussed. The following key conclusions can be drawn from this study:

1. The ~ 40 μm thickness of the deposited coatings on 304 stainless steel shows no major defects. Mo coatings exhibited a relatively uniform composition, around 35% wt.% through the coating thickness areas.
2. TiC and WC coatings increased the microhardness by a factor of 5 and the Mo coating by a factor of 2 relative to the microhardness of the base metal stainless steel. The wear resistance of the WC coating is more than 5 times and that of the TiC and Mo coatings about 2.5 times better than that of stainless steel.
3. Mo coating significantly improves the corrosion resistance in 5% NaCl solutions, which corrode 350 times slower than stainless steel. Phase transformation from austenite to ferrite contributes to the corrosion resistance improvement. TiC coating increased the corrosion resistance with a 10 times slower corrosion rate. WC coating does not show improvement in the corrosion resistance while being compared to the base metal.
4. The corrosion performance of Mo-coated 304 stainless steel decreased at 400 and 650 °C, under both Ar and air atmosphere. Higher temperature resulted in thinner coated thickness and increasing the composition of Mo content. The phase transformation from austenite to ferrite at 400 °C dramatically decreases the corrosion resistance of the Mo-coated sample. The significantly low corrosion potential at 650 °C can be attributed to the formation of intermetallic phase.

Acknowledgments

Financial support from the National Sciences and Engineering Research Council (NSERC), Ontario Centres of Excellence (OCE) and Huys Industries Ltd is gratefully acknowledged. The authors thank TechnoCoat Co., Ltd for materials support. The authors would like to thank Dr. Joyce Koo and Dr. Mehrdad Iravani from University of Waterloo, for wear test experiment and valuable discussions. Mr. Dominic Leung and Kevin Chan from Huys Industries are highly acknowledged for their technical support.

References

1. Z. Chen and Y. Zhou, Surface Modification of Resistance Welding Electrode by Electro-Spark Deposited Composite Coatings: Part I. Coating Characterization, *Surf. Coat. Technol.*, 2006, **201**(3-4), p 1503–1510
2. K.R.C.S. Raju, N.H. Faisal, D.S. Rao, S.V. Joshi, and G. Sundararajan, Electro-Spark Coatings for Enhanced Performance of Twist Drills, *Surf. Coat. Technol.*, 2008, **202**(9), p 1636–1644
3. A.V. Kolomeichenko and I.S. Kuznetsov, Tribotechnical Properties of Electrospark Coatings of Amorphous and Nanocrystalline Iron Alloys, *J. Frict. Wear*, 2014, **35**(6), p 501–504
4. C. Luo, X.A. Xiong, and S.J. Dong, TiB_2/Ni Coatings on Surface of Copper Alloy Electrode Prepared by Electrospark Deposition, *Trans. Nonferrous Met. Soc. China*, 2011, **21**(2), p 317–321
5. A.V. Ribalko, O. Sahin, and K. Korkmaz, A Modified Electrospark Alloying Method for Low Surface Roughness, *Surf. Coat. Technol.*, 2009, **203**(23), p 3509–3515
6. P. Wang, L. Ma, Z.J. Liang, and J.J. Zhao, Preparation and Mechanical Properties of Two Nickel Base Alloy Coatings Achieved by Electrospark Deposition, *Acta Metall. Sin. (Engl. Lett.)*, 2011, **24**(4), p 309–314
7. R.N. Johnson and G.L. Sheldon, Advances in the Electrospark Deposition Coating Process, *J. Vac. Sci. Technol., A*, 1986, **4**(6), p 2740–2746
8. J.S. Wang, H.M. Meng, H.Y. Yu, Z.S. Fan, and D.B. Sun, Wear Characteristics of Spheroidal Graphite Roll WC-8Co Coating Produced by Electro-Spark Deposition, *Rare Met.*, 2010, **29**(2), p 174–179
9. Y.G. Tkachenko, D.Z. Yurchenko, V.F. Britun, L.P. Isaeva, and V.T. Varchenko, Structure and Properties of Wear-Resistant Spark-Deposited Coatings Produced with a Titanium Carbide Alloy Anode, *Powder Metall. Met. C+*, 2013, **52**(5-6), p 306–313
10. S.H. Bae, H.D. Lim, W.J. Jung, W. Gil, E.C. Jeon, S.G. Lee, H.J. Lee, I.S. Kim, and H.W. Lee, A Study on the Mechanical Properties of Duplex Stainless Steel Weldment According to Mo Contents, *Korean J. Met. Mater.*, 2012, **50**(9), p 645–651
11. M.M. Larijani and N. Bafandeh, Corrosion Behaviors of Mo Coating on Stainless Steel 316 Substrates Implanted by Different Nitrogen Ion Fluences, *Eur. Phys. J. Appl. Phys.*, 2014, **65**(3), p 31301
12. A.P. Hammersley, S.O. Svensson, M. Hanfland, A.N. Fitch, and D. Hausermann, Two-Dimensional Detector Software: From Real Detector to Idealised Image or Two-Theta Scan, *High Press. Res.*, 1996, **14**(4-6), p 235–248
13. J.P. Oliveira, R.M. Miranda, N. Schell, and F.M.B. Fernandes, High Strain and Long Duration Cycling Behavior of Laser Welded NiTi Sheets, *Int. J. Fatigue*, 2016, **83**, p 195–200
14. J.P. Oliveira, F.M.B. Fernandes, N. Schell, and R.M. Miranda, Martensite Stabilization During Superelastic Cycling of Laser Welded NiTi Plates, *Mater. Lett.*, 2016, **171**, p 273–276
15. A.A. Burkov, Influence of Carbon Content of WC-Co Electrode Materials on the Wear Resistance of Electrospark Coatings, *J. Surf. Eng. Mater. Adv. Technol.*, 2012, **02**(02), p 65–70
16. A. International, Standard Test Methods for Pitting and Crevice Corrosion Resistance of Stainless Steels and Related Alloys by Use of Ferric Chloride Solution, 2015
17. M.M. Larijani and N. Bafandeh, Corrosion Behaviors of Mo Coating on Stainless Steel 316 Substrates Implanted by Different Nitrogen Ion Fluences, *Eur. Phys. J. Appl. Phys.*, 2014, **65**(3), p 31301
18. H. Demiroren, M. Aksoy, T. Yildiz, and S. Buytoz, The Corrosion Characterization of a Ferritic Stainless Steel with Mo Addition in H2SO4 and HCI, Acid Solutions, *Prot. Met. Phys. Chem.*, 2009, **45**(5), p 628–634
19. S.H. Bae and H.W. Lee, Effect of Mo Contents on Corrosion Behaviors of Welded Duplex Stainless Steel, *Met. Mater. Int.*, 2013, **19**(3), p 563–569
20. H. Hwang and Y. Park, Effects of Heat Treatment on the Phase Ratio and Corrosion Resistance of Duplex Stainless Steel, *Mater. Trans.*, 2009, **50**(6), p 1548–1552

21. H.-Y. Liou, W.-T. Tsai, Y.-T. Pan, and R.-I. Hsieh, Effects of Alloying Elements on the Mechanical Properties and Corrosion Behaviors of 2205 Duplex Stainless Steels, *J. Mater. Eng. Perform.*, 2001, **10**(2), p 231–241
22. J. Padgurskas, R. Kreivaitis, R. Rukuza, V. Mihailov, V. Agafii, R. Kriukiene, and A. Baltusnikas, Tribological Properties of Coatings Obtained by Electro-Spark Alloying C45 Steel Surfaces, *Surf. Coat. Technol.*, 2017, **311**, p 90–97
23. G. Krauss, *Steels: Processing, Structure and Performance*, ASM International, Materials Park, 2005
24. P. Paulraj and R. Garg, Effect of Intermetallic Phases on Corrosion Behavior and Mechanical Properties of Duplex Stainless Steel and Super-Duplex Stainless Steel, *Adv. Sci. Technol. Res.*, 2015, **9**(27), p 87–105
25. A.Y. Chen, W.F. Hu, D. Wang, Y.K. Zhu, P. Wang, J.H. Yang, X.Y. Wang, J.F. Gu, and J. Lu, Improving the Intergranular Corrosion Resistance of Austenitic Stainless Steel by High Density Twinned Structure, *Scr. Mater.*, 2017, **130**, p 264–268
26. H. Bhadeshia and R. Honeycombe, *Steels: Microstructure and Properties*, Elsevier, Amsterdam, 2006
27. G. Fargas, A. Mestra, and A. Mateo, Effect of Sigma Phase on the Wear Behavior of a Super Duplex Stainless Steel, *Wear*, 2013, **303**(1-2), p 584–590
28. Z.Q. Feng, Y.H. Yang, and J. Wang, Effect of Mn Addition on the Precipitation and Corrosion Behaviour of 22% Cr Economical Duplex Stainless Steel After Isothermal Aging at 800 °C, *J. Alloys Compd.*, 2017, **699**, p 334–344